Biochimie 187 (2021) 131–143

Contents lists available at ScienceDirect

Biochimie

journal homepage: www.elsevier.com/locate/biochi

Insights into the structure and function of the C-terminus of SGTs (small glutamine-rich TPR-containing proteins): A study of the *Aedes aegypti* homolog

Natália G. Quel [a, b], Luiz Fernando de C Rodrigues [c], Annelize Z.B. Aragão [a], Glaucia M.S. Pinheiro [a], Rafael P. Camacho [a], Denio E.P. Souto [d], Lauro T. Kubota [a, e], Leandro R.S. Barbosa [c, f], Carlos H.I. Ramos [a, b, *]

[a] Institute of Chemistry, University of Campinas UNICAMP, Campinas SP, 13083-970 Brazil
[b] National Institute of Science & Technology of Structural Biology and Bioimage (INCTBEB), Brazil
[c] Institute of Physics, University of São Paulo, São Paulo SP, 05508-090 Brazil
[d] Department of Chemistry, Federal University of Paraná-UFPR, Curitiba PR, 81530-900, Brazil
[e] National Institute of Science & Technology of Bioanalytics (INCTBio), Brazil
[f] Brazilian Synchrotron Light Laboratory (LNLS), Brazilian Center for Research in Energy and Materials (CNPEM), Campinas, Brazil

ARTICLE INFO

Article history:
Received 1 April 2021
Received in revised form
24 May 2021
Accepted 26 May 2021
Available online 31 May 2021

Keywords:
SGT
Hsp90
Aedes
Protein folding
Protein structure and function

ABSTRACT

SGTs (small glutamine-rich TPR-containing proteins) are dimeric proteins that belong to the class of co-chaperones characterized by the presence of TPR domains (containing tetratricopeptide repeats). Human (SGTA) and yeast (Sgt2) SGTs are characterized by three distinct domains: an N-terminal dimerization domain, a central TPR-domain important for binding to other proteins (chaperones included) and a C-terminal domain involved in hydrophobic interactions. Both these SGTs are involved in the cellular PQC (protein quality control) system, as they interact with chaperones and have functions that aid stress recovery. However, there are differences between them, such as structural features and binding specificities, that could be better understood if other orthologous proteins were studied. Therefore, we produced and characterized a putative SGT protein, designated AaSGT, from the mosquito *Aedes aegypti*, which is a vector of several diseases, such as dengue and Zika. The protein was produced as a folded dimer which was stable up to 40 °C and was capable of binding to AaHsp90 and fully protecting a model protein, α-synuclein, from aggregation. The conformation of AaSGT was investigated by biophysical tools and small angle X-ray scattering, which showed that the protein had an elongated conformation and that its C-terminal domain was mainly disordered. The results with a C-terminal deletion mutant supported these observations. Altogether, these results are consistent with those from other functional SGT proteins and add to the understanding of the PQC system in *Aedes aegypti*, an important aim that may help to develop inhibitory strategies against this vector of neglected diseases.

1. Introduction

A large number of proteins are involved in maintaining proteostasis in the cell [1]. Many of these proteins constitute the PQC (protein quality control) system, which relies on cooperation between chaperones and the proteasome system. Many chaperones, such as Hsp90 and Hsp70, and cochaperones are involved in folding and preventing aggregation under stress conditions. One important cochaperone is SGT (small glutamine-rich TPR-containing protein). SGTs are dimeric proteins and each monomer is composed of an N-

Abbreviations: CD, circular dichroism; DD, dimerization domain; Hsp, heat shock protein; PQC, Protein Quality Control; SAXS, small-angle X-ray scattering; SEC-MALS, size exclusion chromatography coupled to multi-angle light scattering; SGT, small glutamine-rich TPR-containing protein; TPR, tetratricopeptide repeats.

* Corresponding author. Institute of Chemistry, University of Campinas UNICAMP, Campinas SP, 13083-970 Brazil.
E-mail address: cramos@unicamp.br (C.H.I. Ramos).

https://doi.org/10.1016/j.biochi.2021.05.012
0300-9084/

terminal dimerization domain (DD), a TPR domain, which interacts with chaperones, and an unstructured C-terminus, with a glutamine-rich region, which interacts with the hydrophobic region of client proteins. SGT (SGTA in humans or Sgt2 in yeast) interacts with both Hsp90 and Hsp70 [2–4]. SGT stabilizes the Hsp70/ADP/client-protein complex, and mediates the interaction between Hsp90 and Hsp70, during complex formation.

SGT recognizes proteins containing exposed hydrophobic regions and protects them by interaction via its C-terminal domain. Furthermore, SGT interacts with the BAG6/GET (human/yeast nomenclature) complex to target client proteins [5,6], and through this interaction, it participates in (1) degradation associated with the endoplasmic reticulum, which is important for cell survival under stress conditions [7], (2) TA protein (tail-anchored protein) recognition and delivery to the TRC40 complex**,** which acts as the anchor to the endoplasmic reticulum membrane [8–11], and (3) targeting of mislocalized proteins in the cytoplasm, sending them for refolding, repositioning to the correct cell location or degradation by the ubiquitin-proteasome system [12–15]. In addition, SGT can also reverse ubiquitination and stabilize proteins so that it can be targeted to another destination instead of being degraded [16].

Furthermore, it was demonstrated that the silencing of the *sgta* gene by iRNA affects human cell proliferation, preventing cell division and leading to death [17]. Similarly, it has been shown that SGT is essential for cell survival and proliferation of *Leishmania donovani* [18]. Moreover, it has been suggested that the absence of SGT can increase the lifespan of potentially toxic proteins in the cell [13,19]. Based on this, the important role of SGTs in cellular protein homeostasis is evident, which highlights the importance of studying new orthologs of SGTs. In this study, we characterized a novel SGT from *Aedes aegypti*, a mosquito of great importance, especially in tropical countries, where the diseases that it spreads are endemic. The findings indicated that AaSGT had chaperone activity, an elongated conformation and that its C-terminal domain was mainly disordered.

2. Materials and Methods

2.1. Sequence identification and analysis

Genome sequencing of *Aedes aegypti* was finished in 2004 [20] and then improved and reannotated in 2018 [21]. The amino acid sequence of AaSGT was found using the human SGTA amino acid sequence as a template against the *A. aegypti* protein databank using the NCBI BLASTp tool (https://blast.ncbi.nlm.nih.gov/Blast.cgi). The AaSGT orthologs listed in Table S1 were used to perform global alignments using Clustal Omega software [22] and to construct the phylogenetic tree (maximum likelihood tree using the JTT model with 1000 bootstrap replicates in MEGA X). The NCBI BLAST Global Alignment tool (https://blast.ncbi.nlm.nih.gov/Blast.cgi) was used to calculate the identity and similarity between the sequences. SMART software [23] was used to identify AaSGT domains and C-QUARK software (https://zhanglab.ccmb.med.umich.edu/C-QUARK/) was used to construct its models. PrDOS [24], DisEMBL [25] and IUPred [26] were used to predict intrinsically disordered regions.

2.2. Gene synthesis and constructions

The AaSGT coding sequence was optimized for *E. coli* expression and synthesized by Epoch Life Science. The sequence was cloned between the *Nde*I-*Xho*I restriction sites of the pET22b vector to obtain pET22b-AaSGT. To construct the yeast expression plasmids, we used the empty vector SM640 (low copy, URA3 marker, and GAL promoter), linearized by *Eco*RI. Details on the primers, plasmids and cloning methodology are provided in Table S2. To further investigate the role of the C-terminus of AaSGT, site-directed mutagenesis using the QuikChange XL Site-Directed Mutagenesis Kit (Agilent), was performed to create a stop codon that generated pET22b-AaSGT$_{1\text{-}208}$, for which primers (Fw 5′-cgcccgccgctcagcccggcgcg-3′ and Rv 5′-cgcgccgggctgagcggcgggcg-3′) were generated by QuikChange Primer Design (https://www.chem.agilent.com/store/primerDesignProgram.jsp). All constructs were confirmed by Sanger sequencing using plasmid primers (T7 primers for pET22b and M13 primers for SM640).

2.3. Yeast heat sensitivity assay

The yeast *sgt2* knockout strain (*sgt2Δ* - Horizon™, cat.# YSC6273-201923099) was transformed following the LiAc/PEG methodology (Elble, 1992) either using an empty vector (SM640, low copy, URA3 marker and GAL promoter) or using the constructs for Sgt2 and AaSGT expression. The heat sensitivity assay was performed using freshly transformed yeast cells after a round of selection in synthetic complete solid medium lacking uracil (SC−U). Single colonies were cultured overnight in liquid YPD medium and centrifuged, after which the pellets were resuspended in 40 mL of fresh YPD (to yield an initial $A_{600nm} = 0.1$) and grown until the mid-log phase ($A_{600nm} = 0.5–0.7$). At this point, yeast cells were serially diluted (5-fold) in sterile water, and 2.5 μL from each dilution was spotted onto two YPG plates. The control plate was grown at 30 °C for a period of 72 h. The heat-shocked plate was incubated at 40 °C for 72 h, followed by 3 more days of incubation at 30 °C. Then, the colonies were counted, and the data were normalized (relative to the number of *sgt2Δ* empty vector colonies). Six independent experiments were performed and statistically analyzed using one-way ANOVA, followed by Bonferroni's multiple comparison test ($p < 0.05$) using Prism software, version 5.

2.4. Protein purification

AaSGT and AaSGT$_{1\text{-}208}$ were expressed in *E. coli* BL21(DE3) with 0.5 mM IPTG (isopropyl thio-β-D-galactoside) at 37 °C and 200 rpm (Forma Orbital Shaker – Thermo Scientific) for 4 h. Then, the cells were harvested by centrifugation at 2496*g* for 15 min at 4 °C, and the pellet was resuspended in buffer containing 25 mM Tris-HCl, 200 mM NaCl, pH 8 (buffer A) with 30 μg mL^{-1} lysozyme, 1 mM phenylmethylsulfonyl fluoride (PMSF) and 5 U DNAse. The lysis was performed by sonication (Misonix Ultrasonic Liquid Processor, S4000) with an amplitude of 30 W, pulsing for 12 s with an interval of 1.5 min, within a 2 min total process on ice. The lysate was centrifuged at 20000 g for 30 min at 4 °C.

For purification purposes, the supernatant was filtered through a 0.45 μm membrane (Millex® Syringe-driven filter unit, Millipore) and loaded onto a HighQ XK16/20 (GE Healthcare) anionic exchange column previously equilibrated with buffer A. The elution was carried out with a step (200 mM, 350 mM and 1 M) or a linear (0–1 M) NaCl gradient for AaSGT and AaSGT$_{1\text{-}208}$, respectively. Then, the proteins were subjected to size exclusion chromatography in a Superdex 200 XK 26/60 (GE Life Sciences) column previously conditioned with buffer A. The protein expression and purification processes were analyzed by SDS-PAGE, the purity was determined using ImageJ software [27] and the concentration was measured by the method [28] modified by Ref. [29]. AaHsp90 and α-synuclein were expressed and purified as previously described [29,30 with modifications].

2.5. Secondary structure determination and thermodynamics assays

Circular dichroism (CD) measurements were performed using a Jasco J-720 spectropolarimeter with a Peltier-type temperature controller (Jasco Inc., Easton, MD, USA). CD spectra were acquired from 260 to 200 nm in a 2 mm quartz path length cuvette at 20 °C. The protein concentration was 3 μM for both AaSGT and $AaSGT_{1-208}$. The spectra were normalized to the mean residual molar ellipticity ([θ]), and the α-helix content was calculated as previously described [32].

To evaluate the thermodynamics of AaSGT and $AaSGT_{1-208}$ unfolding, CD and differential scanning calorimetry (DSC) were performed. For CD, the experiments were conducted from 20 to 90 °C, increasing 1 °C/min, and then the refolding capability was assessed from 90 to 20 °C, at the same rate. These CD experiments were performed using a 5 mm quartz path length cuvette, and the concentration was 2 μM for both AaSGT and $AaSGT_{1-208}$. For DSC, the experiments were conducted in a MicroCal VP-DSC (Malvern) from 20 to 90 °C at 1 °C/min using 50 and 75 μM AaSGT or $AaSGT_{1-208}$.

2.6. Identification of intracellular SGT and the heat-shock assay

Aedes albopictus C6/36 cells (kindly donated by Prof. Dr. José Luiz Proença Modena, IB/UNICAMP, Brazil) were cultivated in 6-well plates with Eagle's minimum essential medium supplemented with 10% fetal bovine serum at 28 °C and 5% CO_2 until confluent. For the heat-shock assay, the plates were incubated at 37 °C for 90 min [33]. Then, the cells were washed with ice-cold PBS and detached from the plate with trypsin. After that, the cells were washed three times with ice-cold PBS by centrifugation at 1200*g* for 5 min at 4 °C. For lysis, the cells were incubated with RSB-NP40 buffer (1.5 mM $MgCl_2$, 10 mM Tris–HCl, 10 mM NaCl and 1% Igepal CA 630) in the presence of protease inhibitor cocktail (500 μM AEBSF/mL, 150 nM aprotinin/mL, 1 μM E–64 protease inhibitor/mL, 0.5 mM EDTA/mL, 1 μM leupeptin/mL, Calbiochem) for 2 min on ice. Then, the cells were centrifuged at 12000 g for 15 min at 4 °C. Soluble proteins were resuspended in sample buffer, boiled for 5 min and loaded onto SDS-PAGE. Western blot analysis was performed using a nitrocellulose 0.45 μm membrane, and transfer was conducted in a semidry apparatus (Bio-Rad). Rabbit polyclonal anti-AaSGT (1:20000; RheaBiotec) and mouse monoclonal anti-β-actin (1:5000) (Abcam, #ab184220) were used as the primary antibodies. Secondary antibodies were anti-rabbit-HRP and anti-mouse-HRP IgG (1:5000) conjugated to HRP (Abcam). Membranes were revealed using an ECL kit (GE Healthcare) and observed using an Imager 600 instrument (GE Healthcare). Bands were quantified using ImageJ software, and statistical analysis was conducted in GraphPad Prism 5 software using the Student's t-test.

2.7. Surface plasmon resonance (SPR)

The surface plasmon resonance (SPR) technique was used to determine the reaction kinetics and affinity constant (K_D) for the biomolecular interactions discussed in this work, which involved AaHsp90 and AaSGT (or $AaSGT_{1-208}$). The experiments were conducted in an Autolab Sprit instrument (Eco Chemie B. V., The Netherlands), which has attenuated total internal reflection (Kretschmann configuration) as an operation mode [34]. AaHsp90 (0.5 μM) was immobilized on a self-assembled monolayer (SAM), which was formed by the interaction of mercaptoundecanoic acid (11-MUA) on the gold surface (SPR disk) [35]. The terminal carboxyl groups of 11-MUA were activated via an aqueous solution consisting of 100 mM EDC (N-(3 dimethylamino-propyl)-N-ethylcarbodiimidehydrochloride) and 150 mM NHS (N-hydroxysuccinimide) for the formation of NHS ester groups, which allowed covalent binding of AaHsp90 on SAM onto gold (11-MUA/Au). Furthermore, to prevent nonspecific binding, after the immobilization of AaHsp90 on 11-MUA/Au (SAM/Au), the unbound reactive ester groups were deactivated by an aqueous solution consisting of 1 M ethanolamine (EA), pH 8.5, and the excess unbound EA molecules was then removed by successive washing with water. Afterwards, different concentrations of AaSGT (or $AaSGT_{1-208}$) were added to the SPR disk, and protein-protein interactions were assessed in real time. The concentrations used were 5–20 μM AaSGT and 10–25 μM $AaSGT_{1-208}$. The equilibrium constants were obtained by numerical methods with the aid of specific software for the treatment of the SPR data (Trace Drawer, version 1.5 - BioNavis Ltd., Tampere, Finland).

2.8. α-synuclein aggregation assay

To evaluate the ability of AaSGT to protect a client protein from aggregation, α-synuclein was used as the substrate. α-Synuclein (15 μM) was incubated at 42 °C and 250 rpm for 48 h [31 with modifications] with or without AaSGT (2:1, AaSGT: α-synuclein, monomeric concentrations). Thioflavin T (ThT) was then added (1:1, v:v) at a final concentration of 20 μM and measured by fluorescence, with an excitation of 450 nm and an emission from 475 to 550 nm using an Aminco Bowman® Series 2 (SLM-AMINCO) fluorimeter and a 1 cm quartz path length cuvette. The controls were α-synuclein and AaSGT alone, both incubated under the same conditions.

2.9. Hydrodynamic characterization

For analytical size exclusion chromatography (aSEC), 100 μM AaSGT or 125 μM $AaSGT_{1-208}$ was loaded onto Superdex 200 10/300 GL (GE Life Sciences) in buffer A and coupled to an AKTA FPLC system (GE Life Sciences). For calibration purposes, standard proteins with known Stokes radii (R_s) (ovalbumin, aldolase, conalbumin, carbonic anhydrase, ferritin, and thyroglobulin) were used at a concentration of approximately 2 mg mL^{-1}. Blue dextran was used for column void determination. The standard protein elution volumes were used to calculate -$(\log Kav)^{1/2}$, which were plotted against their R_s or hydrodynamic radius to construct the calibration curves. Linear fitting analysis of these calibration curves was applied to find the R_s for AaSGT and $AaSGT_{1-208}$.

Size exclusion chromatography coupled to multiangle light scattering (SEC-MALS) experiments was conducted using an AKTA FPLC instrument (GE Healthcare Life Sciences) coupled to a miniDAWN TREOS light scattering detector and to an Optilab T-rEX refractive index detector (Wyatt Technology). AaSGT and $AaSGT_{1-208}$ were loaded onto Superdex 200 10/300 GL (GE Life Sciences) in buffer A at the same concentrations described for aSEC. Data analysis was performed using Astra 6 software (Wyatt Technology).

Dynamic light scattering (DLS) experiments were conducted in a Malvern Zetasizer Nano ZS 90 (Model 3690) instrument equipped with a 633 nm laser in a polystyrene cell at 20 °C. AaSGT was used at concentrations of 10, 40, 50, 75 and 100 μM, and $AaSGT_{1-208}$ was used at concentrations of 50, 75 and 100 μM.

2.10. SAXS

SAXS data were collected at the SAXS1 beamline in the Brazilian National Laboratory of Synchrotron Light (LNLS, Campinas, São Paulo). The sample consisted of AaSGT or $AaSGT_{1-208}$ in buffer A placed in a sample holder with mica windows at ~1000 mm distance from the detector (2D Pilatus 300 K), allowing a scattering

vector q range ($q = 4\pi/\lambda \sin(2\theta)$, where 2θ is the scattering angle and λ, equal to 1.488 Å, is the radiation wavelength) of $0.15 < q < 3.5$ nm^{-1}. Radiation damage was checked by measuring consecutive short time frames (~10 s) and comparing the scattering curves in the small-q region. No radiation damage was observed in this study. The collected data were azimuthally integrated to obtain one-dimensional scattering profiles, and the buffer contribution was subtracted, taking into account the attenuation of the sample. Data analysis was performed with the ATSAS package [36]. Guinier analysis was performed to obtain the radius of gyration (R_g) and the zero-angle forward scattering intensity (I(0)). The p(r) function was obtained with GNOM software [37] and allowed for the calculation of R_g and I(0). Molecular mass (MM) calculations were performed using Bayesian inference of different concentration independent methods, all of which relied on I(0) value. DAMMIF, DAMAVER and DAMMIN [36,38,39] were used to generate twenty *ab initio* envelopes (with beads as dummy atoms) and average these structures, with subsequent refinement to obtain a final low-resolution structure. Rigid body modeling, with the addition of missing residues, was performed using BUNCH [40] with PDB structures modeled using SWISS-MODEL with previously published crystal structures as templates. Both *ab initio* and rigid body models were aligned using SUPCOMB [41]. Systematic deviations were inspected mainly by means of CorMap and its p-value, following the procedure described by Franke et al. [42]. Molecular mass (MM) was also calculated without having to rely on protein concentration [43]. The first group of methods relied on the Kratky plot, which allows the calculation of the Porod invariant Q_P, which is related to the protein volume and was introduced in SAXSMoW software [44,45] and in the ATSAS package with different adjustments and approaches. Another recent method introduced a new invariant, the volume of correlation (V_c), calculated using the area under the I(q)*q vs q plot, and relating it empirically to R_g to find the MM. This allows more reliable calculations for nonglobular proteins, because the I(q)q *vs.* q plot, integration converges even for disordered proteins [46]. The most recent individual technique on MM calculations employs machine learning on Kratky plots and compares to data from SASBDB [47,48] to predict both D_{max} and MM for the protein [43,49].

3. Results and discussion

3.1. Bioinformatic analysis

The sequence alignment shows that AaSGT shares 29–41% of identity and 44–58% of similarity with its orthologues (Table S3). SGT characteristic domains – namely N-terminal dimerization domain (DD), TPR and the C-terminus, were identified (Fig. 1A and B) and found to be conserved in AaSGT (Fig. S1). DD is comprised of residues 5 to 72, and the residues involved in dimerization are conserved (Fig. S1) [5]. Furthermore, the residues involved in EEVD interactions (both with Hsp70 and Hsp90) are all conserved (Fig. S1) [2,50]. According to the alignments, AaSGT is an *Aedes aegypti* homolog of the proteins Sgt2 and SGTA in yeast and human, respectively. Additionally, the phylogenetic tree (Fig. 1C) shows that AaSGT is evolutionarily close to *Drosophila melanogaster* SGT, which indicates that the results obtained in this work could also be extrapolated to this ortholog and likely to other Diptera SGTs.

The structures of the AaSGT domains were analyzed using three-dimensional predictor c-QUARK (Fig. 2). Fig. 2A shows that DD appears to be organized into 4 helices that are connected by short loops, similar to the structures obtained for its orthologs in human and yeast [5,51]. The TPR domain is composed of three TPR motifs, which are located at residues 85 to 118, 119 to 152 and 153 to 186, and Fig. 2B shows that the TPR domain is organized as expected for this domain, with a helix-turn-helix for each TPR motif. The region that links both the DD and TPR domains is 12 residues long in AaSGT, similar to human SGTA, which is 14 residues long [19], but this is different from that in *Leishmania braziliensis* SGT, which is 61 residues long, and yeast Sgt2, which has an intermediate length of 23 residues [52]. Finally, the C-terminal domain is composed of α-helices and two unstructured regions, one from 204 to 225 and the other from 297 to 327 (Fig. 2C). Similarly, the prediction of disorder (Fig. 2D) confirmed that these two regions are intrinsically disordered. These observations are in accordance with the results from NMR obtained by Ref. [53] for human SGTA, which showed a profile of an unstructured region. Additionally, this was expected since this region is Q- and P-rich (Fig. 1A).

3.2. AaSGT recovers the yeast sgt2Δ phenotype

A yeast knockout of Sgt2 (*sgt2*Δ) shows a greater sensitivity to thermal stress [54,55] but the mechanism by which Sgt2 is involved in yeast survival after severe heat shock remains unclear. We asked whether AaSGT had a similar function and investigated this hypothesis by heat sensitivity assays using a *sgt2*Δ lineage transformed with constructs that allow the inducible expression of the Sgt2 and AaSGT proteins. After severe heat shock (72 h at 40 °C), it was observed that the presence of AaSGT not only recovered the heat resistance phenotype but also was more effective in aiding cell survival (Fig. 3A). Growth recovery was 1.8x when Sgt2 was present and 3.3x when AaSGT was present, compared with *sgt2*Δ (Fig. 3B; six independent experiments using data from the survival of *sgt2*Δ yeast as an internal normalization: *sgt2*Δ = 1).

3.3. Recombinant AaSGT and the deletion mutant were folded and stable

AaSGT was purified to a high purity level (~90%) (Figs. 4A and S2) and was folded (Fig. 4C). The CD spectra show bands at 222 nm and 208 nm, indicating an α-helical protein (Fig. 4C – filled circles). Hence, the AaSGT α-helix content was calculated to be ~60%, which is similar to the high-resolution structures of the DD and TPR domains of its orthologs, since both domains are mainly composed of α-helices (PDB IDs: 4CPG, 4GOD, 2LXB, 2VYI, 5LYP, 4ASV, and 3SZ7) [2,5,51,52,56,57]. Moreover, this percentage of α-helical content is also in accordance with that reported for SGTs from *Caenorhabditis elegans* (58%) [58] and *L. braziliensis* (55%) [4].

The mutant deleted at the C-terminus, $AaSGT_{1\text{-}208}$, was also purified to a high purity level (~90%) (Figs. 4B and S3) and was folded (Fig. 4C). The CD spectra for $AaSGT_{1\text{-}208}$ show bands at 222 nm and 208 nm, indicating an α-helical protein (Fig. 4C – open circles). The α-helical content was ~70%, a higher value than that of the wild-type protein because the deleted region was mainly disordered (Fig. 2D). The CD signal was normalized considering the length of the protein; thus, the percentage of α-helices was higher in the mutant. This result confirmed the predictions showing that the C-terminal region has two disordered regions (Fig. 2C–D).

The raw data for the thermal-induced unfolding of both AaSGT and $AaSGT_{1\text{-}208}$ are shown in Fig. S4, and the analysis is shown in Fig. 5. The CD curve profiles were similar, as both showed stability up to 40 °C followed by a two-state-like transition up to 60 °C (Fig. S4A). A similar CD profile is explained by the unstructured nature of the deleted region that does not form secondary structures. Moreover, the unfolding of both AaSGT and $AaSGT_{1\text{-}208}$ was reversible, as the CD signal was approximately 90% recovered after cooling (data not shown). Thermal-induced unfolding was also analyzed by DSC (Fig. S4A), showing a profile similar to that shown by CD, with a stability up to 40 °C followed by a two-state-like

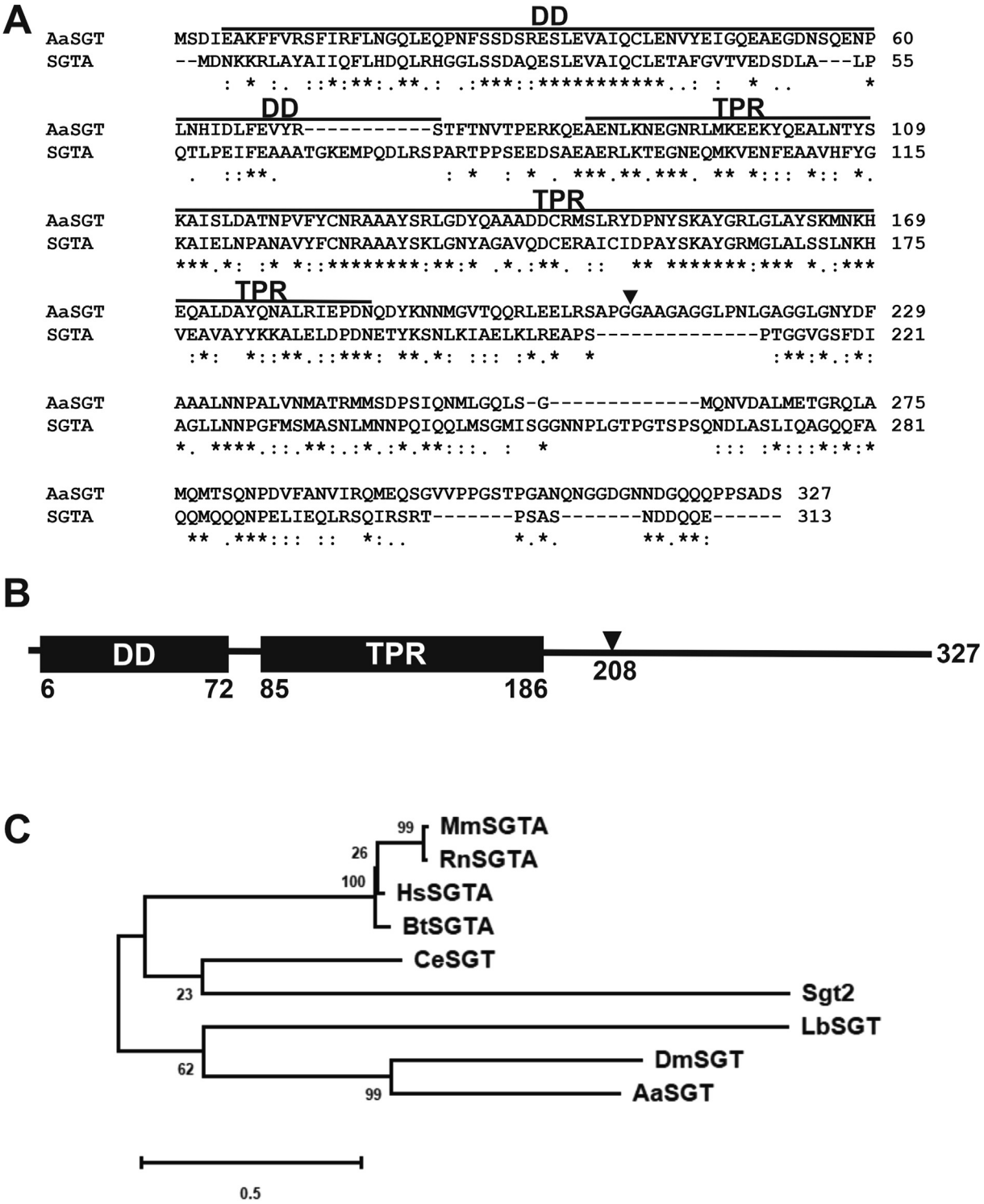

Fig. 1. Sequence analysis. A: Sequence alignment between AaSGT and human SGTA. Dimerization (DD) and TPR domains are identified. An arrowhead indicates the C-terminal residue of $AaSGT_{1\text{-}208}$. Alignment was performed using Clustal Omega software. "*" indicates identical residues, ":" indicates conserved residues with higher similarities, "." indicates conserved residues with lower similarities. **B:** Schematic representation of AaSGT, showing both DD and TPR domains, which were identified using SMART software. An arrowhead indicates position 208 for $AaSGT_{1\text{-}208}$. **C:** Evolutionary analysis by the maximum likelihood method. The evolutionary history was inferred by using the maximum likelihood method and the JTT matrix-based model [68]. The tree with the highest log likelihood (−5445.59) is shown. The percentage of trees in which the associated taxa clustered together is shown next to the branches. Initial tree(s) for the heuristic search were obtained automatically by applying Neighbor-Join and BioNJ algorithms to a matrix of pairwise distances estimated using a JTT model, and then selecting the topology with superior log likelihood value. The tree is drawn to scale, with branch lengths measured in the number of substitutions per site. This analysis involved 9 amino acid sequences and a total of 421 positions were present in the final dataset. Evolutionary analyses were conducted in MEGA X [69].

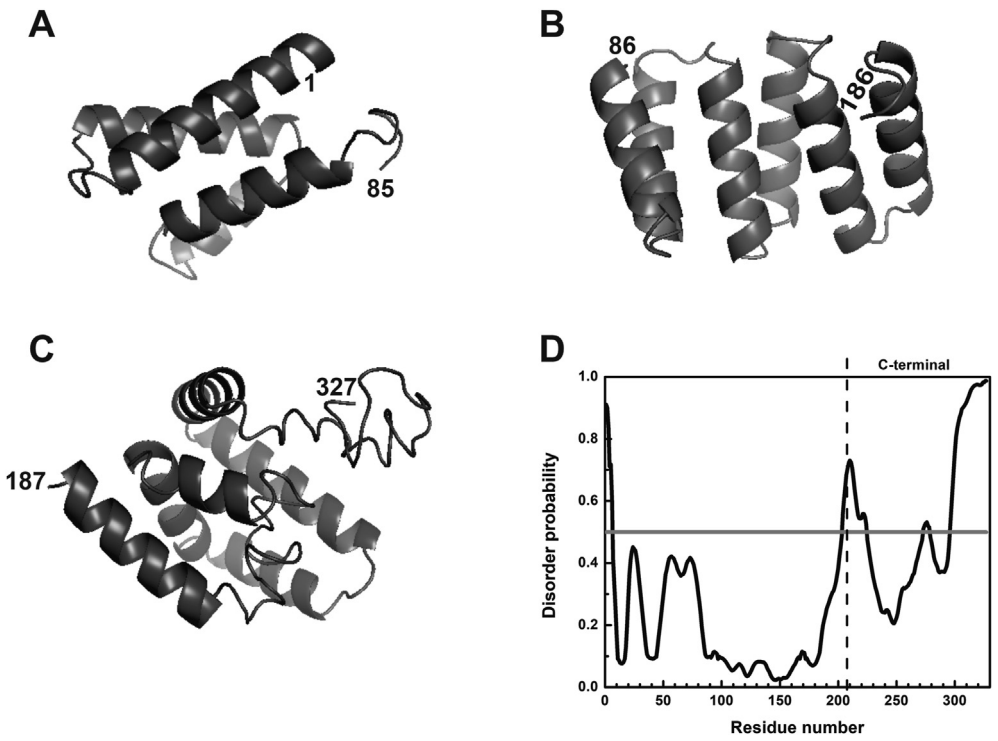

Fig. 2. *In silico* prediction models of AaSGT domains obtained using C-QUARK software. A: N-terminal dimerization domain (DD), residues 1 to 85, organized in 4 helices that are connected by short loops, a composition also shown in its orthologs. **B:** TPR domain, residues 86 to 186, organized in a characteristic helix-turn-helix fashion. **C:** C-terminal domain, residues 187 to 327, showing two unstructured regions, one from 204 to 225 and the other from 297 to 327. The region deleted in $AaSGT_{1\text{-}208}$ is shown in a lighter color. **D:** The prediction of disordered regions confirms that the regions from 204 to 225 and from 297 to 327 are intrinsically disordered.

transition up to 60 °C. A similar DSC profile is explained by the unstructured nature of the deleted region that does not form compacted structures that unfold when the protein melts. Because the data up to 60 °C showed a two-state-like transition, demonstrated no sign of aggregation and revealed reversibility, these two proteins were analyzed together as proteins that had two-state unfolding up to 60 °C (Fig. 5). Therefore, data above 60 °C were not used in the two-state analysis due to aggregation (see voltage inset in Fig. 3A). The two-state analysis showed that the first transition for both wild-type or mutant, measured either by CD or DSC, has a Tm (point at the middle of the transition) of approximately 52 °C ± 1 °C (Table 1). Additionally, DSC analyses indicated a similar enthalpy variation for the unfolding of both the wild-type and the mutant (Table 1). Altogether, the results show that the unstructured nature of the C-terminal region (deleted in the mutant) does not form either secondary structures or compacted structures that unfold when the protein melts.

3.4. *AaSGT is expressed in Aedes cells, binds AaHsp90 and protects α-synuclein from aggregation*

After showing that AaSGT proteins were produced folded and stable, it was important to demonstrate whether the protein had functional activities similar to those of other SGTs. Thus, a series of experimental investigations was performed. Fig. 6 shows the identification of AaSGT in *Aedes albopictus* larval cell extracts for the first time through Western blot analysis using an anti-SGT polyclonal antibody (Fig. 6). The presence of a band recognized by this antibody in the cell extract (Fig. 6A) indicates that this protein is expressed in this cell line under physiological conditions (cells maintained at 28 °C) similar to other SGTs that are constitutively expressed [4,17,18,59,60]. These cells were also exposed to a heat-shock treatment (37 °C for 1.5 h) to evaluate whether AaSGT expression increased under these conditions. As shown in Fig. 6B, there was no significant difference in AaSGT expression levels in either control or heat-shocked cells. Most likely, the heat-shock conditions are not sufficient to induce AaSGT expression, a result supported by previous studies suggesting that SGT participation during heat shock is only required in extreme situations [3,54]. Yeast cells lacking SGT (Δ*sgt2*) are not affected by short-term and mild heat-shock conditions at 42 °C [3]. In contrast, the survival of the Δ*sgt2* strains decreased under more stringent conditions, such as long-term, 3-day, and mild heat-shock conditions at 40 °C [54], or short-term and severe heat-shock conditions at 55 °C [3,54]. A similar evaluation was not possible because *Aedes albopictus* larvae cells do not survive extreme heat-shock conditions.

The interaction between AaSGT (or $AaSGT_{1\text{-}208}$) and AaHsp90 was evaluated using SPR. Fig. S5 shows that the SPR angle (θ_{SPR}) increased with the concentration of both AaSGT and $AaSGT_{1\text{-}208}$ (Fig. S5 A and B, respectively). However, it is possible to observe that the addition of AaSGT at a concentration higher than 15 μM (or 20 μM $AaSGT_{1\text{-}208}$) did not lead to significant differences in the effective $\Delta\theta_{SPR}$. Possibly, saturation of the surface occurred due to a limited number of available binding sites of AaHsp90. For a quantitative study, the equilibrium constants were obtained by numerical methods with the aid of specific software for the treatment of the SPR data (see Materials and Methods). The stoichiometry adopted was 1 to 1 for the reaction between AaHsp90 and AaSGT (or $AaSGT_{1\text{-}208}$). The experimental curves shown in Fig. S5 were fit globally (thin black lines), and the kinetic and thermodynamic parameters were obtained (Table 2). The values show that AaSGT and $AaSGT_{1\text{-}208}$ interact with AaHsp90, and $AaSGT_{1\text{-}208}$ has a 10 times higher affinity than AaSGT (Table 2). This difference might be due to the greater availability of TPR domains in the $AaSGT_{1\text{-}208}$,

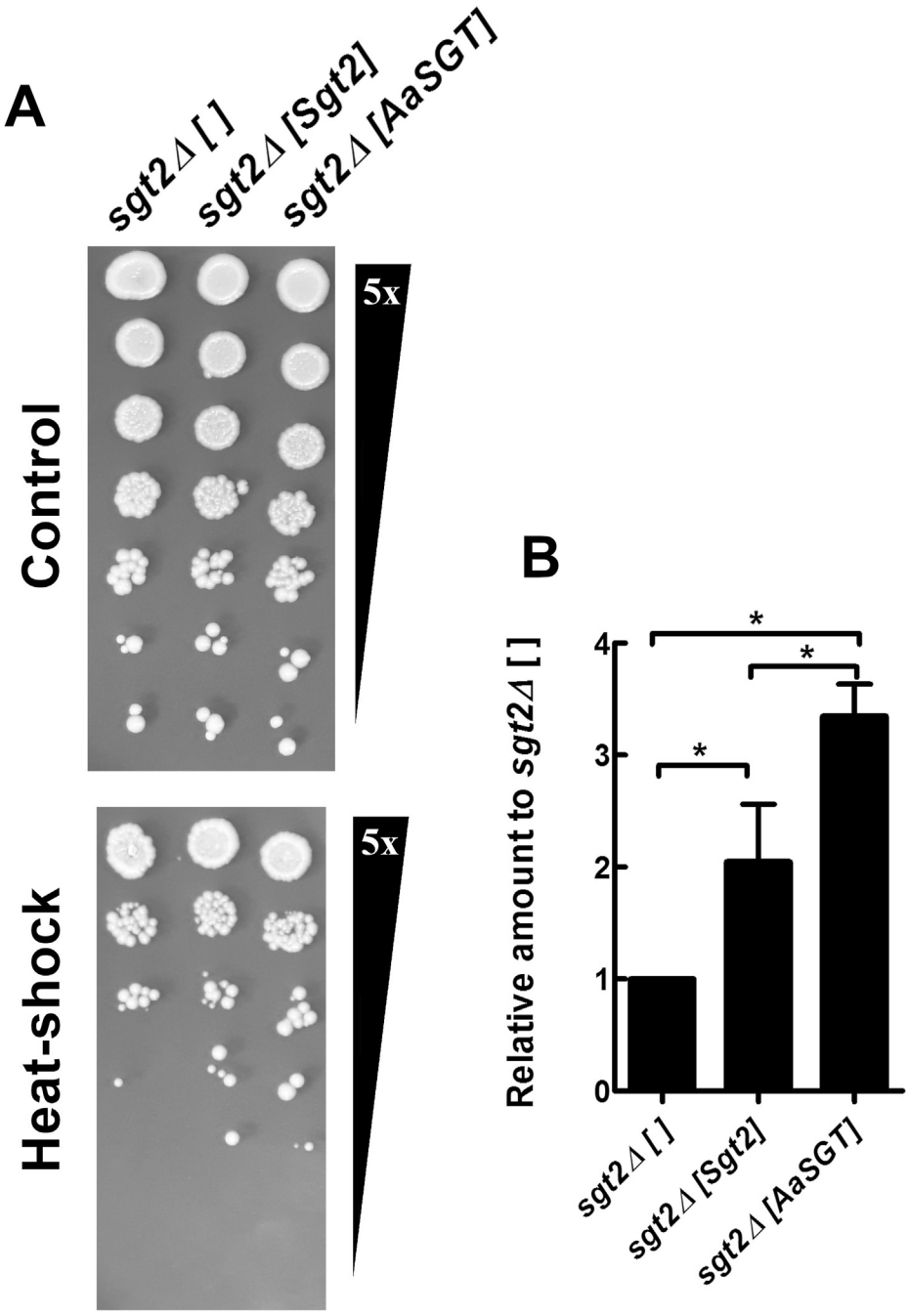

Fig. 3. Phenotype complementation in yeast using a severe heat sensitivity assay. A: Representative experiment showing control (30 °C - upper panel) and heat-shock (40 °C - lower panel) yeast plates. The sgt2Δ strain was transformed with empty vector (sgt2Δ [ ]) or with constructs for the expression of yeast and *Aedes* proteins (sgt2Δ [Sgt2] and sgt2Δ [AaSGT], respectively). Serial dilutions (5-fold) were spotted onto YPG plates. **B:** Six independent experiments were performed; the colonies were counted, and the data were normalized (using data from the *sgt2*Δ yeast survival as an internal normalization: *sgt2*Δ = 1). Bars represent the mean and SD of each transformed yeast (normalized to sgt2Δ [ ] = 1). Statistical significance is indicated by an asterisk ($p < 0.05$).

since in this construction there is no flexible C-terminus that can somehow interfere with the interaction. As a matter of fact, the interactions may be both weak and possibly transient as suggested for SGTs and Hsp90s from other organisms [2–4,58]. Similarly, it has been reported in Ref. [54] that the interaction between Sgt2 and Hsp82 (yeast homologs) were unable to be assessed through pull-down assays, suggesting that the interaction may occur as weak and transient interactions, which corroborates the results using AaSGT and AaHsp90.

SGTs are capable of binding to the exposed hydrophobic regions of client proteins, protecting them from the hydrophilic cytoplasm and preventing their aggregation. Therefore, α-synuclein, a protein whose aggregation is related to disease in humans [46], was used as a substrate to evaluate the ability of AaSGT to protect a client protein from aggregation. α-Synuclein was chosen as a model substrate due to its propensity to aggregate, as it has a hydrophobic region that is involved in membrane anchoring [61]. Fig. 7 shows that AaSGT protected nearly all α-synuclein from aggregation under the conditions used here. Curiously, Sgt2 was not able to protect model proteins from aggregation, unless it was in the presence of

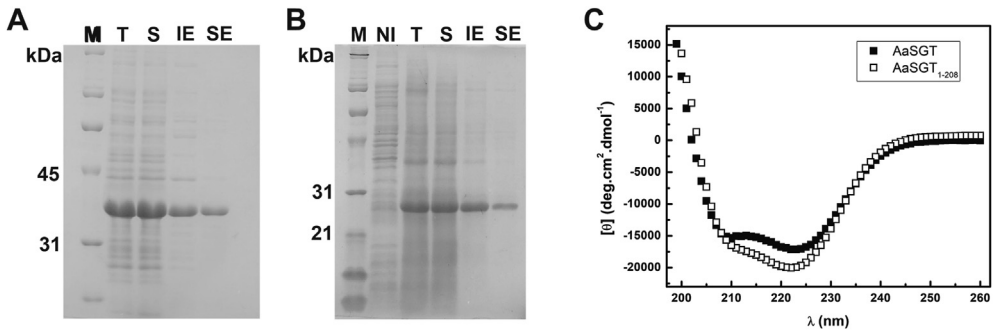

Fig. 4. AaSGT and AaSGT$_{1-208}$ were purified with high purity and were folded. A: Purification steps for AaSGT **(A)** and AaSGT$_{1-208}$ **(B)**. NI: noninduced; M: molecular mass standard, T: total expressed proteins, S: soluble proteins after cell lysis, IE: ion exchange chromatography, SE: size exclusion chromatography. **C:** Circular dichroism spectra of AaSGT (solid circles) and AaSGT$_{1-208}$ (open circles). α-helical content was 60% and 70%, respectively.

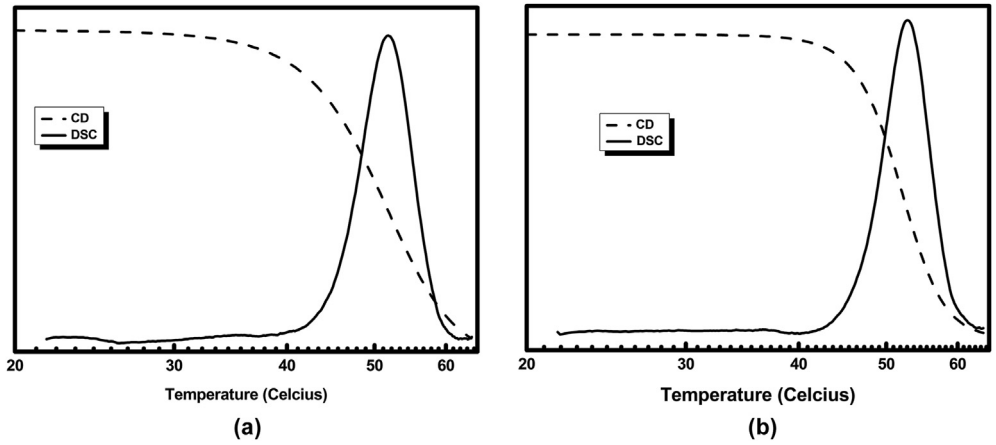

Fig. 5. Characterization of thermodynamic parameters of AaSGT (A) and AaSGT$_{1-208}$ (B). Data from circular dichroism (CD) and differential scanning calorimetry (DSC) were analyzed and fit using a two-state equation. Through this analysis, it is likely that AaSGT behaves in a two-state fashion, at least until residue number 208, since there are no significant differences when comparing the AaSGT and AaSGT$_{1-208}$ unfolding profiles and thermodynamic parameters (described in Table 1). Data above 60 °C were not used in the two-state analysis due to aggregation (data not shown).

Table 1
Thermodynamic parameters obtained for AaSGT and AaSGT$_{1-208}$ through CD and DSC.

Protein	Tm (°C) CD	Tm (°C) DSC	DeltaH (Kcal/mol)	DeltaHv (Kcal/mol)
AaSGT	52 ± 1	51.5 ± 0.2	72.3 ± 4.1	97.5 ± 2.1
AaSGT$_{1-208}$	53 ± 1	52.3 ± 0.1	63.5 ± 0.7	97.0 ± 1.4

Hsp70 [62]. In fact, an increase in turbidity was observed in the presence of Sgt2, likely due to its interaction with the aggregates, indicating that Sgt2 is capable of binding to the client protein but is not able to protect it from aggregation [62]. These findings are in good agreement with the phenotype complementation assay results using Δ*sgt2* yeast strains (shown above), which indicate that AaSGT appears to be more effective than Sgt2 in promoting survival under heat-shock conditions. Altogether, the combined results indicated that AaSGT has the conformational aspects and specified functions of a protein belonging to the SGT family.

3.5. On the conformation of AaSGT: characterization of hydrodynamic parameters

Since AaSGT has the characteristics of a structured and functional protein (see above), a set of experiments was conducted to establish its conformational aspects. First, AaSGT was subjected to SEC-MALS to obtain its molecular mass in solution (Fig. 8A), which was found to be 72.7 ± 0.6 kDa. This molecular mass indicated that the wild-type protein was a dimer, as expected since one of the characteristics of SGTs is the presence of the N-terminal dimerization domain (DD) [4,58,63]. The values of the Stokes radius (R_s) and diffusion coefficient (D) for AaSGT were 45.6 ± 0.4 Å (Figs. 8B) and 4.4 ± 0.4 × 10^{-7} cm^2 s^{-1}, respectively. These values were compared to values calculated for a hypothetical solid nonhydrated sphere with the same molecular mass (Table 3). This comparison, which can also be performed with the Perrin value, is a good estimate of how much the conformation of the protein deviates from a globular shape [64]. The results (Table 3; Perrin factor of 1.7) indicated that the measured parameters were different from those of a sphere and thus that AaSGT had a nonglobular or elongated shape, as observed for its orthologs [4,58,63]. In addition, the AaSGT R_s is in good agreement with those from its orthologs in human, *C. elegans* and *L. braziliensis* [4,58,63].

The hydrodynamic parameters of AaSGT$_{1-208}$ were also characterized. Its molecular mass was determined to be 48.1 ± 0.1 kDa

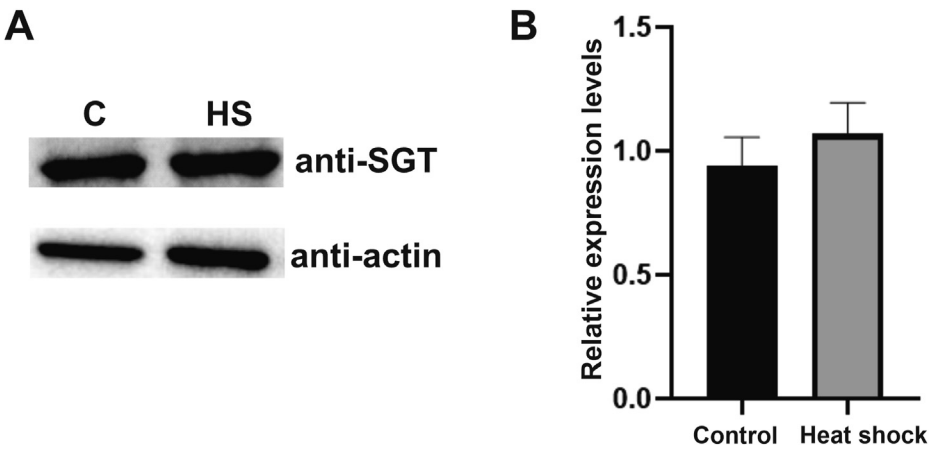

Fig. 6. Identification of AaSGT in *Aedes albopictus* C636 larvae cell extracts and evaluation of heat shock treatment on protein expression. A: Western blot analysis using an anti-SGT polyclonal antibody. C: control cells, HS: heat-shocked cells (37 °C for 1.5 h). An anti-actin antibody was used as a loading control for normalization purposes. **B:** Relative expression of AaSGT in both control and heat-shocked cells (37 °C for 1.5 h) showing that there was no significant difference in expression levels. Bars represent the mean and SD of three experiments.

Table 2
Kinetic parameters obtained via SPR from the AaSGT (or $AaSGT_{1\text{-}208}$) and AaHsp90 interaction: k_a: association kinetic constant; k_d: dissociation kinetic constant; K_D: equilibrium dissociation constant (affinity constant).

Reaction	k_a (L $mol^{-1}s^{-1}$)	k_d (s^{-1})	K_D (mol L^{-1})	X^2 (chi^2)
AaSGT − AaHsp90	2.76×10^{2}	8.56×10^{-4}	3.10×10^{-6}	8.76
$AaSGT_{1\text{-}208}$ − AaHsp90	2.36×10^{1}	7.56×10^{-4}	3.21×10^{-5}	5.49

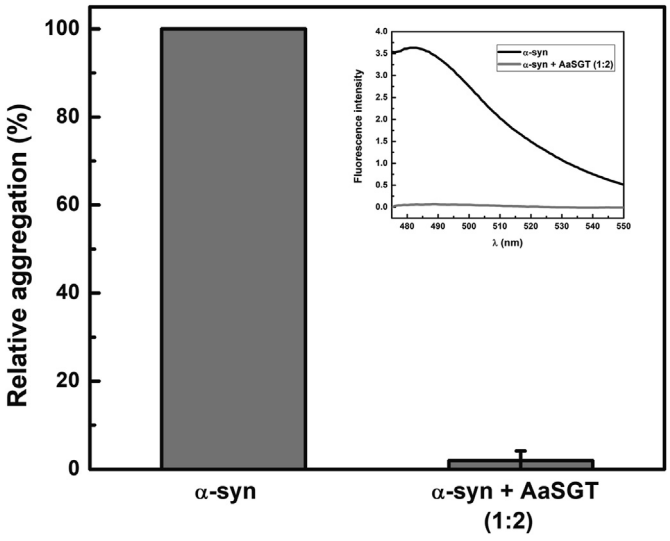

Fig. 7. Protection of α-synuclein from aggregation. AaSGT protected nearly all α-synuclein from aggregation under the conditions used here. Bar represents the mean with SD of three independent experiments. Inset: curves of thioflavin T fluorescence intensity for α-synuclein in the presence (gray line) or absence (black line) of AaSGT.

(Fig. 8C), indicating that the mutant exists as a dimer, as expected since one of the characteristics of SGTs is the presence of the N-terminal dimerization domain (DD) [4,58,63]. The values of R_s and D for $AaSGT_{1\text{-}208}$ were 37.4 ± 0.3 Å (Figs. 8D) and $5.6 \pm 0.2 \times 10^{-7}$ cm^2 s^{-1} (Table 3), respectively, which is in good agreement with a smaller protein compared to wild-type AaSGT but is still compact. Moreover, the obtained R_s is in good agreement with that reported for the SGTA mutant lacking the C-terminal region [63]. The Perrin factor of 1.6 and the other results (Table 3) indicated that the mutant had a nonglobular or elongated shape. The results support the structural models shown in Fig. 2 and the calculations by SAXS (see below).

3.6. On the conformation of AaSGT: SAXS

SAXS is an important tool to assess protein size, molecular mass, shape and flexibility at a low-medium resolution [65], and was used to compare both AaSGT and $AaSGT_{1\text{-}208}$. Fig. 9A shows the scattering curves of both AaSGT and $AaSGT_{1\text{-}208}$, along with the respective Guinier plot (inset). The SAXS curves for both proteins are quite different, clearly indicating different structural conformations in solution. Guinier analysis (inset, Fig. 9A) allows for the calculation of R_g and I(0), which are directly related to particle size and molecular weight, respectively. In this case, the R_g values were calculated as 4.41 ± 0.11 nm and 2.79 ± 0.01 nm for AaSGT and $AaSGT_{1\text{-}208}$, respectively. The molecular masses calculated by Bayesian inference of the individual methods were 78.5 kDa and 42.9 kDa for dimeric AaSGT and $AaSGT_{1\text{-}208}$, respectively, which are in good agreement with those expected from the sequences and measured by SEC-MALS (Tables 3 and 4).

A scattering particle shape can be assessed employing the p(r) function (Fig. 9B), with its Fourier transform (GNOM fit) represented along with the experimental data (Fig. 9A). The p(r) profiles highlight the globular shape of $AaSGT_{1\text{-}208}$ and an average elongated shape for AaSGT, which may also be related to an increased degree of flexibility. The p(r) function can also be used to calculate R_g and I(0), so a comparison of these values with those obtained from Guinier analysis is a useful validation of the obtained maximum particle distance (D_{max}) and function profile. The values obtained for D_{max} are 15.5 ± 0.5 nm and 9.5 ± 0.5 nm for AaSGT and $AaSGT_{1\text{-}208}$, respectively. Table 4 indicates compatible parameter values by both Guinier and p(r) analyses. The $AaSGT_{1\text{-}208}$ dimensionless Kratky profile (inset of Fig. 9B) has a more bell-like shape than that of AaSGT and has peak positions at (x, y) = (1.82, 1.14),

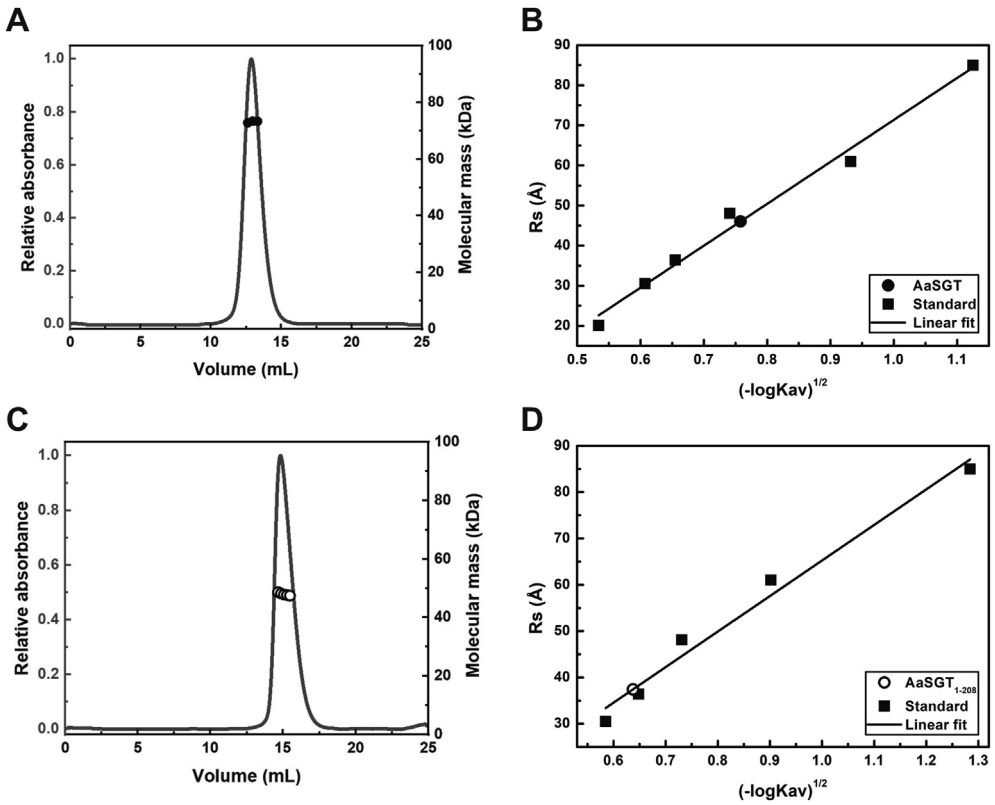

Fig. 8. Characterization of hydrodynamic parameters of AaSGT (A and B) and AaSGT$_{1-208}$ (C and D). A: SEC-MALS analysis to obtain the AaSGT molecular mass in solution. AaSGT was eluted at 12.8 mL, and its molecular mass was determined at 72.7 ± 0.6 kDa, which indicates that the wild-type protein is a dimer in solution**. B:** aSEC analysis to determine the AaSGT Stokes radius (R_s), which was determined to be 45.6 ± 0.4 Å. Standard proteins were used for calibration purposes: ovalbumin, aldolase, conalbumin, carbonic anhydrase, ferritin and thyroglobulin. **C:** SEC-MALS analysis to obtain the AaSGT$_{1-208}$ molecular mass in solution. AaSGT$_{1-208}$ was eluted at 14.8 mL, and its molecular mass was determined to be 48.1 ± 0.1 kDa, which indicates that the mutant protein is a dimer. **D:** aSEC analysis to determine AaSGT$_{1-208}$ R, which was determined to be 37.4 ± 0.3 Å. Standard proteins used for calibration purposes were the same as those used for AaSGT.

Table 3
Hydrodynamic parameters obtained for AaSGT and AaSGT$_{1-208}$ compared with those predicted for a nonhydrated sphere with the same molecular mass.

	AaSGT (experimental)	AaSGT (predicted)	AaSGT$_{1-208}$ (experimental)	AaSGT$_{1-208}$ (precited)
R_s (Å)	45.6 ± 0.4	27.4[a]	37.4 ± 0.3	24.0[a]
D (x 10^{-7} cm^2 s^{-1})	4.4 ± 0.4	9.0[a]/4.92[b]	5.6 ± 0.2	10.2[a]/6.42[b]

[a] Predicted for a hypothetical solid non-hydrated sphere with the same molecular mass of dimeric AaSGT or AaSGT$_{1-208}$.
[b] Predicted by Hydropro sotware using the homology model as a template.

which indicates that the protein is more compact in solution, whereas AaSGT likely exhibits folded domains with flexible linkers by the deviation from the AaSGT$_{1-208}$ curve, approaching a more disordered profile [66,67]. This indicates again that the C-terminal domain may have a more disordered structure relevant for the protein function.

Both *ab initio* and rigid body models were employed to obtain the protein envelope for both AaSGT and AaSGT$_{1-208}$ and to obtain the domain orientation of PDB files with the inclusion of missing residues. For rigid body modeling, P2 symmetry was imposed, and contact restraints were applied according to previous findings [5]. Both approaches are compared in terms of fitting and of the final models in Fig. 9D. Visual inspection and CorMap p-values (Table 4) indicate a better fit for the envelopes calculated by the *ab initio* approach, but rigid body simulations still gave an interesting view of how the domains may be oriented relative to each other. The models obtained for both AaSGT and AaSGT$_{1-208}$ were validated via comparison to the experimental translational coefficient diffusion, D, as shown in Table 3. The measured D value for wild-type AaSGT was 4.4 × 10^{-7} cm^2 s^{-1}, whereas for the SAXS model it was 4.9 × 10^{-7} cm^2 s^{-1}. The measured D value for mutant AaSGT was 5.6 × 10^{-7} cm^2 s^{-1}, while that for the SAXS model was 6.4 × 10^{-7} cm^2 s^{-1}. As the values are similar, we can assume that the obtained models are indeed the most likely conformation of these proteins. Moreover, since the R_g/R_h ratio is higher than 0.775 for both AaSGT and AaSGT$_{1-208}$, this indicates that the proteins have a nonspherical or elongated shape, as discussed above for the hydrodynamic parameters.

4. Conclusion

Sequence similarity is a powerful tool to identify gene orthologs, although needs confirmation via the characterization of the expressed protein. The combination of these two strategies was used to recognize AaSGT as a protein belonging to the SGT family. This recognition was possible via the structural and conformational characteristics provided by the experiments in this study. AaSGT was identified in *Aedes* cells and found to be capable of binding the

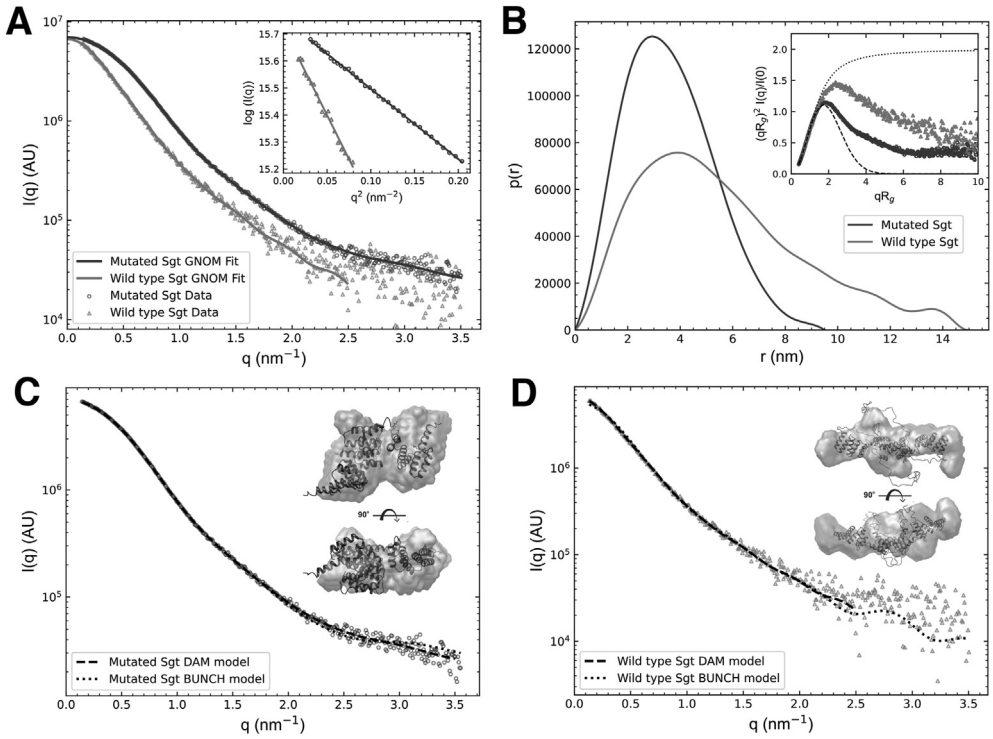

Fig. 9. SAXS analysis for both AaSGT and AaSGT$_{1-208}$. A: Scattering data points for AaSGT$_{1-208}$ (blue) and AaSGT (red), with p(r) fits (solid lines). *Inset*, Guinier plots with linear fits. **B)** p(r) functions obtained by GNOM, with dimensionless Kratky plots in the *inset*. **C)** *Ab initio* (p-value = 0.012) and rigid body (p-value = 6×10^{-6}) models for AaSGT$_{1-208}$. **D)** *Ab initio* (p-value = 0.035) and rigid body (p-value < 10^{-6}) models for AaSGT. Three-dimensional reconstructions are superimposed for comparison. Missing residues of the rigid body model are represented by loops.

Table 4
SAXS structural parameters.

	AaSGT$_{1-208}$	AaSGT
Guinier R_g (nm)	2.79 ± 0.01	4.41 ± 0.11
Guinier I(0) (10^6 AU)	6.96 ± 0.01	6.74 ± 0.05
MM_{Qp} (kDa)[a]	42.3	90.5
$MM_{SAXSMoW}$ (kDa)[a]	44.4	77.5
MM_{Vc} (kDa)[a]	43.2	77.0
$MM_{S\&S}$ (kDa)[a]	48.3	120.0
MM_{Bayes} (kDa)	42.9[b]	78.5[c]
$MM_{Sequence}$ dimer (kDa)	47.9	72.0
p(r) R_g (nm)	2.81 ± 0.01	4.47 ± 0.05
p(r) I(0) (10^6 AU)	6.96 ± 0.01	6.68 ± 0.07
D_{max} (nm)	9.5 ± 0.5	15.5 ± 0.5

[a] Calculated using the I(0) value obtained by Guinier analysis.
[b] Most probable value, with 32.1% probability. Interval of [40.7, 45.2] kDa, with 91.8% probability.
[c] Most probable value, with 25.3% probability. Interval of [75.3, 87.0] kDa, with 91.7% probability.

Hsp90 chaperone from *Aedes* and of protecting a model protein from aggregation. Additionally, a construct expressing AaSGT was capable of increasing the survival of the Δ*sgt2* yeast strain better than the complementation by Sgt2 itself.

The study of other ortholog proteins may help to understood differences between SGTs, mainly the most studies from human and yeast. They seem to share similarities regarding the disordered C-terminus but differ in the extension of the region that links both the DD and TPR domains, shorter in AaSGT (12 residues long) and human SGTA (14 residues long [19]), but longer in *Leishmania braziliensis* SGT (61 residues long [4]) and in yeast Sgt2 (23 residues long [52]) what may result in differences in the dynamic conformation of the dimer. Nonetheless, all have an elongated shape [4,58,63] and are constitutively expressed [4,17,18,59,60] as AaSGT did. However, AaSGT appeared to be more effective than Sgt2 in promoting survival under heat-shock conditions. Different from yeast Sgt2 [62], AaSGT protected nearly all α-synuclein from aggregation under the conditions used here, and was more effective in aiding cell survival.

Several biophysical tools used in this work confirmed the dimeric nature of AaSGT from its molecular mass. Dimerization is attributed to the N-terminal domain, and in the models created by SAXS, these domains are in the center of the dimer, while the TPR domain, which is involved in binding the MEEVD motif of Hsp90, is adjacent to the dimerization domain. Even in the absence of the C-terminal domain, the DD-TPR dimer is nonglobular, as shown by the measurements of the hydrodynamic parameters of the deletion mutant and their comparison with that of a sphere with the same mass of the dimer. The models constructed by SAXS support these results. Furthermore, the full-length protein, even with a disordered C-terminus, was also found to be elongated by all experimental investigations used in this work.

When compared with the DD and TPR domains, much less information on the conformation of the C-terminal domains of SGTs is available, which challenges the understanding of the binding of the cochaperone with client proteins. The results from AaSGT deleted for the C-terminus compared with those from wild-type AaSGT strongly indicated that the C-terminus is disordered, as supported by the predictions made using its sequence. The C-terminal regions lack sufficient secondary structure or packing to affect the thermal-induced unfolding investigation conducted using CD and DSC under the conditions tested in this work. These findings are supported by a recent NMR and mutational study [53] showing that the C-terminal region has poor peak dispersion characteristic of an unfolded conformation.

The general conclusion is that the SGT from *Aedes* was identified *in vivo* for the first time. The protein has functional features that suggest it has a role in mosquito cellular proteostasis by preventing protein misfolding and improving survival in stress situations. *Aedes aegypti* is a vector of viruses that cause serious diseases in humans, and knowledge of its proteins may help the development of strategies to eliminate these diseases.

Authorship contribution

N.G.Q.: Data collection, analysis and interpretation. D.E.P.S. and L.T.K.: SPR (data collection, analysis and interpretation). A.Z.B.A.: Clonning and Yeast experiments (data collection, analysis and interpretation). R.P.C.: alfa-synuclein experiment. *G.M.S.P., L.R.S.B., L.F.C.R.*: SAXS (data collection, analysis and interpretation). *L.F.C.R., C.H.I.R.*: Data analysis and interpretation. *C.H.I.R.*: designed the work. *All authors*: drafted and critically reviewed the article.

Competing interest statement

The authors declare no competing interests.

Acknowledgements

This work was partially supported by FAPESP (2015/15822-1, 2012/01953-9, 2016/05019-0) and CNPq to LRSB who also holds a research fellowship from CNPq (306943/2015-8, 420567/2016-0). CHIR has a research fellowship from CNPq and FAPESP (2017/26131-5). NGQ received fellowships from FAPESP (2014/25967-4). LFCR received fellowship from CAPES (88887.508861/2020-00). Molecular graphics and analyses performed with UCSF Chimera, developed by the Resource for Biocomputing, Visualization, and Informatics at the University of California, San Francisco, with support from NIH P41-GM103311. This research used facilities of the Brazilian Synchrotron Light Laboratory (LNLS), part of the Brazilian Center for Research in Energy and Materials (CNPEM), a private non-profit organization under the supervision of the Brazilian Ministry of Science, Technology and Innovations (MCTI). The SAXS1 beamline staff is acknowledged for the assistance during the experiments (proposals 20170202 and 20190061). The authors also thank Prof. Dr. J. L. P. Módena for gently providing C636 cells and J. Amaro for technical assistance.

Appendix A. Supplementary data

Supplementary data to this article can be found online at https://doi.org/10.1016/j.biochi.2021.05.012.

References

[1] A.O. Tiroli-Cepeda, C.H.I. Ramos, An overview of the role of molecular chaperones in protein homeostasis, Protein Pept. Lett. 18 (2011) 101–109, https://doi.org/10.2174/092986611794475093.

[2] E.M. Krysztofinska, N.J. Evans, A. Thapaliya, J.W. Murray, R.M.L. Morgan, S. Martinez-lumbreras, R.L. Isaacson, Structure and interactions of the TPR domain of Sgt2 with yeast chaperones and Ybr137wp, Front. Mol. Biosci. 4 (2017) 68, https://doi.org/10.3389/fmolb.2017.00068.

[3] P.C. Angeletti, D. Walker, A.T. Panganiban, Small glutamine-rich protein/viral protein U–binding protein is a novel cochaperone that affects heat shock protein 70 activity, Cell Stress Chaperones 7 (2002) 258–268, doi.org/10.1379/1466-1268(2002)007<0258:sgrpvp>2.0.co;2.

[4] A.L.S. Coto, T. V Seraphim, F.A.H. Batista, P.R. Dores-silva, A.B.F. Barranco, F.R. Teixeira, L.M. Gava, J.C. Borges, Structural and functional studies of the Leishmania braziliensis SGT co-chaperone indicate that it shares structural features with HIP and can interact with both Hsp90 and Hsp70 with similar afinities, Int. J. Biol. Macromol. 118 (2018) 693–706, https://doi.org/10.1016/j.ijbiomac.2018.06.123.

[5] J.W. Chartron, D.G. Vandervelde, W.M. Clemons, Structures of the Sgt2/SGTA dimerization domain with the get5/ubl4a UBL domain reveal an interaction that forms a conserved dynamic interface, Cell Res. 2 (2012) 1620–1632, https://doi.org/10.1016/j.celrep.2012.10.010.

[6] P. Leznicki, Q.P. Roebuck, L. Wunderley, A. Clancy, E.M. Krysztofinska, R.L. Isaacson, J. Warwicker, B. Schwappach, S. High, The association of BAG6 with SGTA and tail-anchored proteins, PloS One 8 (2013), e59590, https://doi.org/10.1371/journal.pone.0059590.

[7] Y. Xu, M. Cai, Y. Yang, L. Huang, Y. Ye, SGTA recognizes a noncanonical ubiquitin-like domain in the bag6-Ubl4A-trc35 complex to promote endoplasmic reticulum-associated degradation, Cell Rep. 2 (2012) 1633–1644, https://doi.org/10.1016/j.celrep.2012.11.010.

[8] F. Wang, E.C. Brown, G. Mak, J. Zhuang, V. Denic, A chaperone cascade sorts proteins for posttranslational membrane insertion into the endoplasmic reticulum, Mol. Cell. 40 (2010) 159–171, https://doi.org/10.1016/j.molcel.2010.08.038.

[9] M. Schuldiner, J. Metz, V. Schmid, V. Denic, M. Rakwalska, H.D. Schmitt, B. Schwappach, J.S. Weissman, The GET complex mediates insertion of tail-anchored proteins into the ER membrane, Cell 134 (2008) 634–645, https://doi.org/10.1016/j.cell.2008.06.025.

[10] F. Vilardi, M. Stephan, A. Clancy, A. Janshoff, B. Schwappach, WRB and CAML are necessary and sufficient to mediate tail-anchored protein targeting to the ER membrane, PloS One 9 (2014), e85033, https://doi.org/10.1371/journal.pone.0085033.

[11] Y. Yamamoto, T. Sakisaka, Molecular machinery for insertion of tail-anchored membrane proteins into the endoplasmic reticulum membrane in mammalian cells, Mol. Cell. 48 (2012) 387–397, https://doi.org/10.1016/j.molcel.2012.08.028.

[12] J.D. Roberts, A. Thapaliya, S. Martínez-Lumbreras, E.M. Krysztofinska, R.L. Isaacson, Structural and functional insights into small, glutamine-rich, tetratricopeptide repeat protein alpha, Front. Mol. Biosci. 2 (2015), https://doi.org/10.3389/fmolb.2015.00071.

[13] L. Wunderley, P. Leznicki, A. Payapilly, S. High, SGTA regulates the cytosolic quality control of hydrophobic substrates, J. Cell Sci. 127 (2014) 4728–4739, https://doi.org/10.1242/jcs.155648.

[14] J. Casson, M. Mckenna, S. High, On the road to nowhere: cross-talk between post-translational protein targeting and cytosolic quality control, Biochem. Soc. Trans. 44 (2016) 796–801, https://doi.org/10.1042/BST20160045.

[15] T. Hessa, A. Sharma, M. Mariappan, H.D. Eshleman, E. Gutierrez, R.S. Hegde, Protein targeting and degradation are coupled for elimination of mislocalized proteins, Nature 475 (2012) 394–397, https://doi.org/10.1038/nature10181.Protein.

[16] P. Leznicki, S. High, SGTA antagonizes BAG6-mediated protein triage, Proc. Natl. Acad. Sci. U.S.A. 109 (2012) 19214–19219, https://doi.org/10.1073/pnas.1209997109.

[17] M. Winnefeld, J. Rommelaere, C. Czepluch, The human small glutamine-rich TPR-containing protein is required for progress through cell division, Exp. Cell Res. 293 (2004) 43–57, https://doi.org/10.1016/j.yexcr.2003.09.028.

[18] G. Ommen, M. Chrobak, J. Clos, The co-chaperone SGT of *Leishmania donovani* is essential for the parasite's viability, Cell Stress Chaperones 15 (2010) 443–455, https://doi.org/10.1007/s12192-009-0160-7.

[19] R. Benarroch, J.M. Austin, F. Ahmed, R.L. Isaacson, The roles of cytosolic quality control proteins , SGTA and the BAG6 complex, in: Disease, first ed., Elsevier Inc., 2019 https://doi.org/10.1016/bs.apcsb.2018.11.002.

[20] D.W. Severson, D.L. Knudson, M.B. Soares, B.J. Loftus, *Aedes aegypti* genomics, Insect Biochem. Mol. Biol. 34 (2004) 715–721, doi.org/0.1016/j.ibmb.2004.03.024.

[21] R. Hall, V.S. Joardar, A.K. Jones, R.G.G. Kay, V.K. Kodali, J. Lee, G.J. Lycett, S.N. Mitchell, J. Muehling, M.R. Murphy, A.D. Omer, F.A. Partridge, P. Peluso, B.J. White, L. Zhao, E.L. Aiden, A.R. Hastie, J. Korlach, D.E. Neafsey, A.M. Phillippy, L.B. Vosshall, C.S. Mcbride, Improved reference genome of *Aedes aegypti* informs arbovirus vector control, Nature 563 (2018) 501–507, https://doi.org/10.1038/s41586-018-0692-z.

[22] F. Madeira, Y. mi Park, J. Lee, N. Buso, T. Gur, N. Madhusoodanan, P. Basutkar, A.R.N. Tivey, S.C. Potter, R.D. Finn, R. Lopez, The EMBL-EBI search and sequence analysis tools APIs in 2019, Nucleic Acids Res. 47 (2019) W636–W641, https://doi.org/10.1093/nar/gkz268.

[23] J. Schultz, F. Milpetz, P. Bork, C.P. Ponting, SMART, a simple modular architecture research tool: identification of signaling domains, Proc. Natl. Acad. Sci. Unit. States Am. 95 (1998) 5857–5864, https://doi.org/10.1073/pnas.95.11.5857.

[24] T. Ishida, K. Kinoshita, PrDOS: prediction of disordered protein regions from amino acid sequence, Nucleic Acids Res. 35 (2007), https://doi.org/10.1093/nar/gkm363.

[25] R. Linding, L.J. Jensen, F. Diella, P. Bork, T.J. Gibson, R.B. Russell, Russell Protein disorder prediction: implications for structural proteomics, Structure 11 (2003), https://doi.org/10.1016/j.str.2003.10.002.

[26] B. Mészáros, G. Erdős, Z. Dosztányi, IUPred2A: context-dependent prediction of protein disorder as a function of redox state and protein binding, Nucleic Acids Res. 46 (2018) W329–W337, https://doi.org/10.1093/nar/gky384.

[27] C.A. Schneider, W.S. Rasband, K.W. Eliceiri, NIH Image to ImageJ: 25 years of image analysis, Nat. Methods 9 (2012) 671–675, https://doi.org/10.1038/nmeth.2089.

[28] H. Edelhoch, Spectroscopic determination of tryptophan and tyrosine in proteins, Biochemistry 6 (1967) 1948–1954, https://doi.org/10.1021/bi00859a010.

[29] C.N. Pace, F. Vajdos, L. Fee, G. Grimsley, T. Gray, How to measure and predict

the molar absorption-coefficient of a protein, Protein Sci. 4 (1995) 2411–2423, https://doi.org/10.1002/pro.5560041120.
[30] N.G. Quel, G.M.S. Pinheiro, L.F. de C. Rodrigues, L.R.S. Barbosa, W.A. Houry, C.H.I. Ramos, Heat shock protein 90 kDa (Hsp90) from *Aedes aegypti* has an open conformation and is expressed under heat stress, Int. J. Biol. Macromol. 156 (2020) 522–530, https://doi.org/10.1016/j.ijbiomac.2020.04.029.
[31] W. Hoyer, T. Antony, D. Cherny, G. Heim, T.M. Jovin, V. Subramaniam, Dependence of a-synuclein aggregate morphology on solution conditions, J. Mol. Biol. 322 (2002) 383–393, https://doi.org/10.1016/S0022-2836(02)00775-1.
[32] D.H.A. Correa, C.H.I. Ramos, The use of circular dichroism spectroscopy to study protein folding, form and function, Afr. J. Biochem. Res. 3 (2009) 164–173, https://doi.org/10.5897/AJBR.9000245.
[33] M.G.C. Carvalho, M.A. Rebello, Induction of heat shock proteins during the growth of *Aedes albopictus* cells, Insect Biochem. 17 (1987) 199–206, https://doi.org/10.1016/0020-1790(87)90160-0.
[34] J. Homola, Surface plasmon resonance sensors for detection of chemical and biological species, Chem. Rev. 108 (2008) 462–493, https://doi.org/10.1021/cr068107d.
[35] D. Souto, A. Faria, H. de Andrade, L. Kubota, Using QCM and SPR for the kinetic evaluation of the binding between a new recombinant chimeric protein and specific antibodies of the visceral leishmaniasis, Curr. Protein Pept. Sci. 16 (2015) 782–790, https://doi.org/10.2174/1389203716666150505230416.
[36] D. Franke, M.V. Petoukhov, P.V. Konarev, A. Panjkovich, A. Tuukkanen, H.D.T. Mertens, A.G. Kikhney, N.R. Hajizadeh, J.M. Franklin, C.M. Jeffries, D.I. Svergun, Atsas 2.8: a comprehensive data analysis suite for small-angle scattering from macromolecular solutions, J. Appl. Crystallogr. 50 (2017) 1212–1225, https://doi.org/10.1107/S1600576717007786.
[37] D.I. Svergun, Determination of the regularization parameter in indirect-transform methods using percentual criteria, J. Appl. Crystallogr. 25 (1992) 495–503, https://doi.org/10.1107/S0021889892001663.
[38] D.I. Svergun, Restoring low resolution structure of biological macromolecules from solution scattering using simulated annealing, Biophys. J. 76 (1999) 2879–2886, https://doi.org/10.1016/S0006-3495(99)77443-6.
[39] V.V. Volkov, D.I. Svergun, Uniqueness of ab initio shape determination in small-angle scattering, J. Appl. Crystallogr. 36 (2003) 860–864, https://doi.org/10.1107/S0021889803000268.
[40] M.V. Petoukhov, D.I. Svergun, Global rigid body modeling of macromolecular complexes against small-angle scattering data, Biophys. J. 89 (2005) 1237–1250, https://doi.org/10.1529/biophysj.105.064154.
[41] M.B. Kozin, D.I. Svergun, Automated matching of high- and low-resolution structural models, J. Appl. Crystallogr. 34 (2001) 33–41, https://doi.org/10.1107/S0021889800014126.
[42] D. Franke, C.M. Jeffries, D.I. Svergun, Correlation Map, a goodness-of-fit test for one-dimensional X-ray scattering spectra, Nat. Methods 12 (2015) 419–422, https://doi.org/10.1038/nmeth.3358.
[43] D.I. Hajizadeh, , N. R., D. Franke, C.M. Jeffries, Svergun, Consensus Bayesian assessment of protein molecular mass from solution X-ray scattering data, Sci. Rep. 8 (2018) 7204, https://doi.org/10.1038/s41598-018-25355-2.
[44] I. Fischer, , H. D. O. N., M.D. Oliveira Neto, H.B. Napolitano, A.F. Craievich Polikarpov, Determination of the molecular weight of proteins in solution from a single small-angle X-ray scattering measurement on a relative scale, J. Appl. Crystallogr. 43 (2010) 101–109, https://doi.org/10.1107/S0021889809043076.
[45] V. Piiadov, E. Ares de Araújo, M. Oliveira Neto, A.F. Craievich, I. Polikarpov, SAXSMoW 2.0: online calculator of the molecular weight of proteins in dilute solution from experimental SAXS data measured on a relative scale, Protein Sci. 28 (2019) 454–463, https://doi.org/10.1002/pro.3528.
[46] R.P. Rambo, J.A. Tainer, Accurate assessment of mass, models and resolution by small-angle scattering, Nature 496 (2013) 477–481, https://doi.org/10.1038/nature12070.
[47] E. Valentini, A.G. Kikhney, G. Previtali, C.M. Jeffries, D.I. Svergun, SASBDB, a repository for biological small-angle scattering data, Nucleic Acids Res. 43 (2015) D357–D363, https://doi.org/10.1038/nature12070.
[48] A.G. Kikhney, C.R. Borges, D.S. Molodenskiy, C.M. Jeffries, D.I. Svergun, SASBDB: towards an automatically curated and validated repository for biological scattering data, Protein Sci. 29 (2020) 66–75, https://doi.org/10.1002/pro.3731.
[49] D. Franke, C.M. Jeffries, D.I. Svergun, Machine learning methods for X-ray scattering data analysis from biomacromolecular solutions, Biophys. J. 114 (2018) 2485–2492, https://doi.org/10.1016/j.bpj.2018.04.018.
[50] C. Scheufler, A. Brinker, G. Bourenkov, S. Pegoraro, L. Moroder, H. Bartunik, F.U. Hartl, I. Moarefi, Structure of TPR domain–peptide complexes: critical elements in the assembly of the hsp70–hsp90 multichaperone machine, Cell 101 (2000) 199–210, https://doi.org/10.1016/S0092-8674(00)80830-2.
[51] A.C. Simon, P.J. Simpson, R.M. Goldstone, E.M. Krysztofinska, J.W. Murray, S. High, R.L. Isaacson, Structure of the Sgt2/Get5 complex provides insights into GET-mediated targeting of tail-anchored membrane proteins, Proc. Natl. Acad. Sci. U.S.A. 110 (2013) 1327–1332, https://doi.org/10.1073/pnas.1207518110.
[52] J.W. Chartron, G.M. Gonzalez, W.M. Clemons, A structural model of the Sgt2 protein and its interactions with chaperones and the get4/get5 complex, J. Biol. Chem. 286 (2011) 34325–34334, https://doi.org/10.1074/jbc.M111.277798.
[53] S. Martínez-lumbreras, E.M. Krysztofinska, A. Thapaliya, A. Spilotros, D. Matak-vinkovic, E. Salvadori, P. Roboti, Y. Nyathi, J.H. Muench, M.M. Roessler, D.I. Svergun, S. High, R.L. Isaacson, Structural Complexity of the Co-chaperone SGTA : a Conserved C-Terminal Region Is Implicated in Dimerization and Substrate Quality Control, vol. 6, 2018, pp. 1–18, https://doi.org/10.1186/s12915-018-0542-3.
[54] C. Kohl, P. Tessarz, K. Von Der, R. Zahn, B. Bukau, A. Mogk, Cooperative and independent activities of Sgt2 and Get5 in the targeting of cooperative and independent activities of Sgt2 and Get5 in the targeting of tail-anchored proteins, Biol. Chem. 392 (2011) 601–608, https://doi.org/10.1515/BC.2011.066.
[55] K. Arhzaouy, M. Ramezani-Rad, Nuclear import of UBL-domain protein Mdy2 is required for heat-induced stress response in *Saccharomyces cerevisiae*, PloS One 7 (2012), e52956.
[56] J.F. Darby, E.M. Krysztofinska, P.J. Simpson, A.C. Simon, P. Leznicki, N. Sriskandarajah, D.S. Bishop, L.R. Hale, C. Alfano, M.R. Conte, S. Martínez-Lumbreras, A. Thapaliya, S. High, R.L. Isaacson, Solution structure of the SGTA dimerisation domain and investigation of its interactions with the ubiquitin-like domains of BAG6 and UBL4A, PloS One 9 (2014), e113281, https://doi.org/10.1371/journal.pone.0113281.
[57] S. Dutta, Y. Tan, Structural and functional characterization of human SGT and its interaction with vpu of the human immunodeficiency virus type 1, Biochemistry 47 (2008) 10123–10131, https://doi.org/10.1021/bi800758a.
[58] L.J. Worrall, M.A. Wear, A.P. Page, M.D. Walkinshaw, Cloning, purification and characterization of the *Caenorhabditis elegans* Small Glutamine-rich Tetratricopeptide repeat-containing protein, Biochim. Biophys. Acta 1784 (2008) 496–503, https://doi.org/10.1016/j.bbapap.2007.12.003.
[59] E. Kordes, L. Savelyeva, M. Schwab, J. Rommelaere, J. Jauniaux, C. Cziepluch, Isolation and characterization of human SGT and identification of homologues in *Saccharomyces cerevisiae* and *Caenorhabditis elegans*, Genomics 52 (1998) 90–94, https://doi.org/10.1006/geno.1998.5385.
[60] C. Cziepluch, E. Kordes, M.Y. Poirey, A. Grewenig, J. Rommelaere, J. Jauniaux, Identification of a novel cellular TPR-containing protein, SGT, that interacts with the nonstructural protein NS1 of parvovirus H-1, J. Virol. 72 (1998) 4149–4156, https://doi.org/10.1128/JVI.72.5.4149-4156.1998.
[61] V.N. Uversky, Neuropathology, biochemistry, and biophysics of a-synuclein aggregation, J. Neurochem. 103 (2007) 17–37, https://doi.org/10.1111/j.1471-4159.2007.04764.x.
[62] H. Cho, S. Shan, Substrate relay in an Hsp 70-cochaperone cascade safeguards tail-anchored membrane protein targeting, EMBO J. 37 (2018), e99264, https://doi.org/10.15252/embj.201899264.
[63] S. Liou, C. Wang, Small glutamine-rich tetratricopeptide repeat-containing protein is composed of three structural units with distinct functions, Arch. Biochem. Biophys. 435 (2005) 253–263, https://doi.org/10.1016/j.abb.2004.12.020.
[64] J.C. Borges, C.H.I. Ramos, Analysis of molecular targets of Mycobacterium tuberculosis by analytical ultracentrifugation, Curr. Med. Chem. 18 (2011) 1276–1285, https://doi.org/10.2174/092986711795029537.
[65] D.I. Svergun, M.H. Koch, Small-angle scattering studies of biological macromolecules in solution, Rep. Prog. Phys. 66 (2003) 1735, https://doi.org/10.1088/0034-4885/66/10/R05.
[66] D. Durand, C. Vivès, D. Cannella, J. Pérez, E. Pebay-Peyroula, P. Vachette, F. Fieschi, NADPH oxidase activator p67phox behaves in solution as a multi-domain protein with semi-flexible linkers, J. Struct. Biol. 169 (2010) 45–53, https://doi.org/10.1016/j.jsb.2009.08.009.
[67] V. Receveur-Bréchot, D. Durand, How random are intrinsically disordered proteins? A small angle scattering perspective, Curr. Protein Pept. Sci. 13 (2012) 55–75, https://doi.org/10.2174/138920312799277901.
[68] D.T. Jones, W.R. Taylor, J.M. Thornton, The rapid generation of mutation data matrices from protein sequences, Comput. Appl. Biosci. 8 (1992) 275–282, https://doi.org/10.1093/bioinformatics/8.3.275.
[69] S. Kumar, G. Stecher, M. Li, C. Knyaz, K. Tamura, X. Mega, Molecular evolutionary genetics analysis across computing platforms, Mol. Biol. Evol. 35 (2018) 1547–1549, https://doi.org/10.1093/molbev/msy096.